ACS Catalysis

Research Article

pubs.acs.org/acscatalysis

Terms of Use

Highly Selective Production of Hydrogen Peroxide on Graphitic Carbon Nitride (g-C_3N_4) Photocatalyst Activated by Visible Light

Yasuhiro Shiraishi,*[,†] Shunsuke Kanazawa,[†] Yoshitsune Sugano,[†] Daijiro Tsukamoto,[†] Hirokatsu Sakamoto,[†] Satoshi Ichikawa,[‡] and Takayuki Hirai[†]

[†]Research Center for Solar Energy Chemistry and Division of Chemical Engineering, Graduate School of Engineering Science, Osaka University, Toyonaka 560-8531, Japan

[‡]Institute for NanoScience Design, Osaka University, Toyonaka 560-8531, Japan

Supporting Information

ABSTRACT: Photocatalytic production of hydrogen peroxide (H_2O_2) on semiconductor catalysts with alcohol as a hydrogen source and molecular oxygen (O_2) as an oxygen source is a potential method for safe H_2O_2 synthesis because the reaction can be carried out without the use of explosive H_2/O_2 mixed gases. Early reported photocatalytic systems, however, produce H_2O_2 with significantly low selectivity (~1%). We found that visible light irradiation (λ > 420 nm) of graphitic carbon nitride (g-C_3N_4), a polymeric semiconductor, in an alcohol/water mixture with O_2 efficiently produces H_2O_2 with very high selectivity (~90%). Raman spectroscopy and electron spin resonance analysis revealed that the high H_2O_2 selectivity is due to the efficient formation of 1,4-endoperoxide species on the g-C_3N_4 surface. This suppresses one-electron reduction of O_2 (superoxide radical formation), resulting in selective promotion of two-electron reduction of O_2 (H_2O_2 formation).

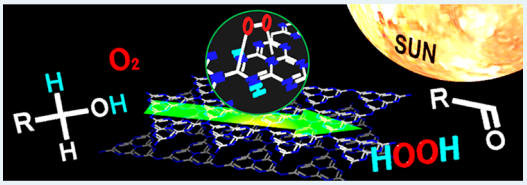

KEYWORDS: *photocatalysis, hydrogen peroxide, visible light, surface chemistry, reduction*

INTRODUCTION

Hydrogen peroxide (H_2O_2) is a clean oxidant that emits only water as a byproduct and is widely used in industry for organic synthesis, pulp bleaching, and disinfection. At present, H_2O_2 is commercially produced by the anthraquinone method,[1] which has some nongreen features, such as high energy utilization, because of the multistep hydrogenation and oxidation reactions. Recently, direct production of H_2O_2 with H_2 and O_2 gases has been studied extensively with Pd[2−4] or Au−Pd bimetallic catalysts.[5−7] This direct synthesis can be an alternative process for H_2O_2 synthesis from the viewpoint of green chemistry, although some care is necessary for operation because of the explosive nature of H_2/O_2 mixed gases.

Photocatalytic H_2O_2 production on semiconductor materials such as titanium dioxide (TiO_2) has also been studied extensively.[8−11] The reactions are usually carried out by UV irradiation (λ < 400 nm) of an O_2-saturated water with TiO_2 in the presence of alcohols as the electron and proton donor. Photoexcitation of TiO_2 produces the electron (e^-) and positive hole (h^+) pairs. The h^+ oxidize alcohol and produce aldehyde and protons, whereas the e^- promote two-electron reduction of O_2 and produce H_2O_2.

$$R{-}CH_2OH + 2h^+ \rightarrow R{-}CHO + 2H^+ \quad (1)$$

$$O_2 + 2H^+ + 2e^- \rightarrow H_2O_2 \quad (2)$$

The reaction proceeds without H_2 gas at room temperature and atmospheric pressure, therefore, a clean and safe H_2O_2 synthesis. Its efficiency is, however, very low because the selectivity for the amount of H_2O_2 formed relative to the amount of alcohol consumed is less than 1%.[8−11] Several kinds of TiO_2 catalysts modified with fluoride[12] or loaded with Au[13] or Au−Ag alloy nanoparticles[14] have been proposed; however, all of these systems exhibit insufficient H_2O_2 selectivity. This is because one-electron reduction of O_2 occurs predominantly and produces a superoxide anion (eq 3).[15] This suppresses two-electron reduction of O_2 (eq 2), resulting in insufficient H_2O_2 selectivity.

$$O_2 + H^+ + e^- \rightarrow {}^{\bullet}OOH \quad (3)$$

Another reason for the low H_2O_2 selectivity is that the formed H_2O_2 is subsequently decomposed by absorbing UV light (~400 nm).[16] Efficient H_2O_2 production, therefore, requires selective promotion of two-electron reduction of O_2 and suppression of subsequent photodecomposition of the formed H_2O_2.

Graphitic carbon nitride (g-C_3N_4) is a metal-free polymeric photocatalyst, with a graphitic stacking structure of the C_3N_4 layers consisting of tri-*s*-triazine units connected through amino groups (Scheme 1).[17,18] This material is successfully activated by the irradiation of visible light (~480 nm) and exhibits high photocatalytic activity for H_2 or O_2 evolution from water[19] and degradation of organic pollutants.[20] Electrochemical analysis of g-C_3N_4 revealed that the bottom of its conduction band is −1.3

Received: December 17, 2013
Revised: January 14, 2014
Published: January 21, 2014

Scheme 1. (a) Graphitic Stacking Structure of g-C_3N_4 Sheet and (b) Photograph of the Prepared g-C_3N_4[a]

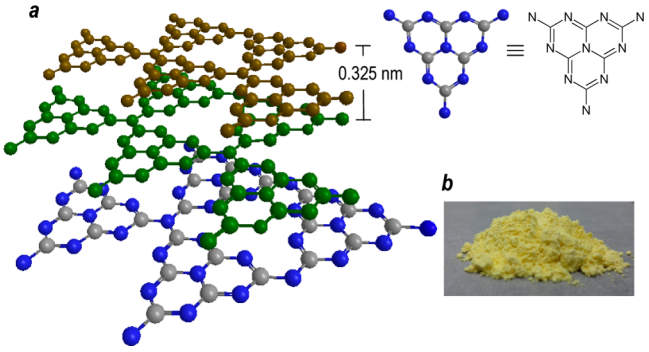

[a]The gray and blue spheres are the C and N atoms, respectively, and the second and third layers of the sheets are green and brown, respectively.

V (vs NHE),[21] which is more negative than the reduction potential of O_2 (−0.28 V vs NHE).[22] This suggests that, as reported,[23−26] g-C_3N_4 is able to promote the reduction of O_2 under visible light irradiation.

Here, we report that g-C_3N_4 activated by visible light in water with alcohol and O_2 selectively promotes two-electron reduction of O_2 while suppressing subsequent photodecomposition of the formed H_2O_2. This thus facilitates highly efficient production of H_2O_2 with more than 90% selectivity. Raman spectroscopy and electron spin resonance (ESR) analysis revealed that selective two-electron reduction of O_2 on the photoexcited g-C_3N_4 is due to the efficient formation of 1,4-endoperoxide species on its surface, which is selectively transformed to H_2O_2.

RESULTS AND DISCUSSION

The g-C_3N_4 photocatalyst was simply prepared by calcination of cyanamide[27] as yellow powders (Scheme 1b). As shown in Figure 1a, the obtained powders (BET surface area, 10.3 m^2 g^{-1}) show strong absorption in the visible region; its band gap is 2.62 eV (= 474 nm). The X-ray diffraction (XRD) pattern of g-C_3N_4 (Figure S1, Supporting Information) shows a distinctive signal assigned to the (002) packing of the C_3N_4 layers at 2θ = 27.4 (d = 0.325 nm).[28] X-ray photoelectron spectroscopy (XPS) of g-C_3N_4 (Figure S2, Supporting Information) shows a C 1s peak at 288 eV assigned to the N=C−N_2 groups of the triazine ring and a N 1s peak at 398−399 eV assigned to the sp^2-hybridized N atoms (C=N−C).[29] The transmission electron microscopy (TEM) image of g-C_3N_4 shows a sheet-like structure (Figure S3, Supporting Information), as often observed for related materials.[30] These data suggest that, as shown in Scheme 1a, g-C_3N_4 indeed possesses a stacking structure of the C_3N_4 layers consisting of tri-*s*-triazine units.

Photocatalytic reactions were performed with ethanol (EtOH) as the electron and proton donor. An EtOH/water mixture (9/1 v/v, 5 mL) containing catalyst (20 mg) was photoirradiated by a Xe lamp (λ > 420 nm) with magnetic stirring under O_2 atmosphere (1 atm) at 298 K. Table 1 summarizes the results obtained by 12 h of photoreaction with the respective catalysts. It must be noted that all of the systems produce acetaldehyde as the main photooxidation product of EtOH, along with minor amounts of acetic acid and CO_2 (mass balance > 95%). With bare TiO_2 (entry 1), the amount of H_2O_2 formed is <0.2 μmol, although a large amount of acetaldehyde (83 μmol) is produced. The selectivity for the amount of H_2O_2 formed relative to the amounts of photooxidation products (= [H_2O_2]/[acetaldehyde + acetic acid + (CO_2)/2] × 100) is <0.2%, suggesting that two-electron reduction of O_2 does not occur selectively.

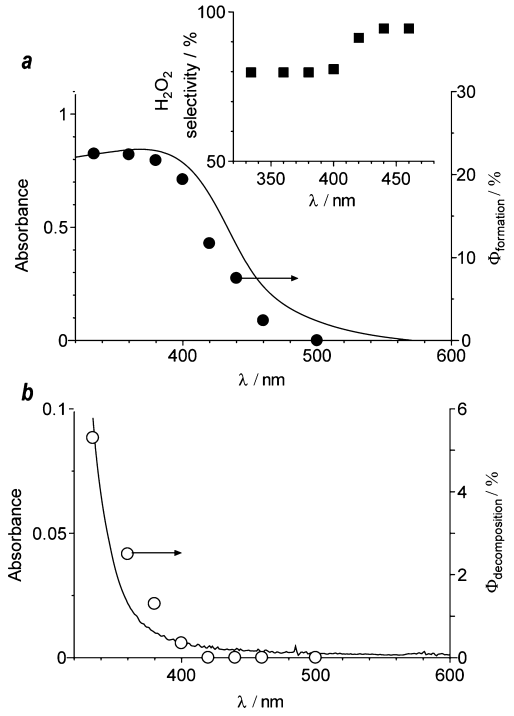

Figure 1. (a) Absorption spectrum of g-C_3N_4 and action spectrum for H_2O_2 formation. Apparent quantum yield for H_2O_2 formation was calculated with the equation {$\Phi_{formation}$ (%) = ([H_2O_2 formed] × 2)/[photon number entered into the reaction vessel] × 100}. The inset shows the change in H_2O_2 selectivity as a function of excitation wavelength. (b) Absorption spectrum of H_2O_2 (420 μM) and action spectrum for H_2O_2 decomposition calculated using the equation {$\Phi_{decomposition}$ (%) = [H_2O_2 decomposed]/[photon number entered into the reaction vessel] × 100}.

As shown by entry 2, TiO_2 loaded with 1 wt % Pt particles (Pt_1/TiO_2) produces a much larger amount of aldehyde (>0.1 mmol) because of the enhanced charge separation by the creation of a Schottky barrier;[31] however, the H_2O_2 selectivity scarcely changes (<0.1%). In addition, TiO_2 loaded with Au particles[32] or modified with fluoride (entries 3 and 4), which has been proposed for H_2O_2 production,[12,13] still shows very low H_2O_2 selectivity (~6.3%). Furthermore, nitrogen-doped TiO_2, a well-known visible light-responsive catalyst,[33] is also ineffective for H_2O_2 formation (entry 5). In contrast, as shown by entry 6, photoreaction with g-C_3N_4 produces a very large amount of H_2O_2 (30 μmol) with significantly high selectivity (90%). This indicates that g-C_3N_4 specifically promotes two-electron reduction of O_2 and facilitates selective H_2O_2 production. It is noted that oxidation of water by the photoformed hole on the semiconductor surface is also a possible mechanism for H_2O_2 formation.[34] In the present g-C_3N_4 system, visible light irradiation in pure water with O_2 scarcely produces H_2O_2 (<0.2 μmol), although the reaction with EtOH produces a much larger amount of H_2O_2 (30 μmol, entry 6). This clearly suggests that oxidation of water by the photoformed hole scarcely contributes to the H_2O_2 production,

dx.doi.org/10.1021/cs401208c | ACS Catal. 2014, 4, 774−780

Table 1. Results for Photocatalytic Production of H_2O_2 from EtOH and O_2 with Various Catalysts[a]

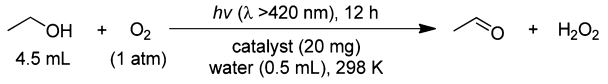

entry	catalyst[b]	H_2O_2/μmol[c]	CH_3CHO/μmol[d]	CH_3COOH/μmol[d]	CO_2/μmol[d]	H_2O_2 selectivity/%[e]
1	TiO_2[f]	<0.2	83	0.1	3.4	<0.2
2	Pt_1/TiO_2[g]	<0.2	188	3.6	3.0	<0.1
3	Au_1/TiO_2[g]	3.0	47	N.D.	1.5	6.3
4	F-TiO_2	<0.2	50	N.D.	1.4	<0.4
5	N-TiO_2	<0.2	23	N.D.	2.1	<0.8
6	g-C_3N_4	30	32	0.7	1.5	90
7	$Pt_{0.1}$/g-C_3N_4[g]	4.2	38	N.D.	1.9	11
8	Pt_1/g-C_3N_4[g]	1.2	308	6.7	5.6	0.4

[a]Photoirradiation was carried out with a 2 kW Xe lamp (light intensity at 420−500 nm was 26.9 W m^{-2}). [b]The subscript texts (M_x) denote the amount of metal loaded on the support (x = wt %). [c]Determined by redox titration with $KMnO_4$ (detection limit: 0.2 μmol). [d]Determined by GC. [e]= $[H_2O_2]/([CH_3CHO] + [CH_3COOH] + [CO_2]/2) \times 100$. [f]JRC-TIO-4 TiO_2 supplied from the Catalyst Society of Japan (equivalent to Degussa P25; particle size, 24 nm; BET surface area, 57 m^2 g^{-1}; anatase/rutile = ca. 83/17). [g]Average diameters of metal particles determined by TEM observations are 3.1 ± 1.1 nm (Pt_1/TiO_2), 3.4 ± 0.9 nm (Au_1/TiO_2), 2.3 ± 0.5 nm ($Pt_{0.1}$/g-C_3N_4), and 4.9 ± 2.2 nm (Pt_1/g-C_3N_4), respectively (see Figure S4, Supporting Information).

leaving that two-electron reduction of O_2 is the main mechanism for H_2O_2 formation.

Figure S5 (Supporting Information) shows time-dependent change in the amount of products during photoreaction of an EtOH/water/O_2 system with g-C_3N_4. Even after prolonged photoirradiation (~24 h), the H_2O_2 selectivity is unchanged (~90%), and the rate of H_2O_2 formation is almost constant. In addition, as shown in Table S1 (Supporting Information), use of other aliphatic or benzylic alcohols also exhibits high H_2O_2 selectivity (ca. 90%). These data suggest that g-C_3N_4 activated by visible light with alcohol selectively produces H_2O_2.

Figure 1a (black circle) shows the action spectrum for H_2O_2 formation, obtained by photoreaction of an EtOH/water/O_2 system with g-C_3N_4 under irradiation of monochromatic light.[35] The apparent quantum yield for H_2O_2 formation ($\Phi_{formation}$) almost agrees with the absorption spectrum of g-C_3N_4, indicating that photoexcitation of g-C_3N_4 promotes H_2O_2 formation. The inset of Figure 1a shows the change in H_2O_2 selectivity as a function of excitation wavelength. Irradiation with >400 nm light shows high H_2O_2 selectivity (>90%), but the selectivity decreases with <400 nm light irradiation. This is because the formed H_2O_2 is decomposed by absorbing UV light.[16] Figure 1b (white circle) shows the action spectrum for H_2O_2 decomposition obtained by photoirradiation of a water (3 mL) containing H_2O_2 (18 μmol) with O_2 at 298 K. The apparent quantum yield for decomposition ($\Phi_{decomposition}$) agrees with the absorption spectrum of H_2O_2 and increases significantly with <400 nm light irradiation. The result is consistent with the decreased H_2O_2 selectivity by <400 nm light irradiation (Figure 1a, inset). These data clearly suggest that photoexcitation of g-C_3N_4 by visible light suppresses subsequent photodecomposition of H_2O_2 and facilitates selective H_2O_2 formation.

In the present g-C_3N_4 system, reaction temperature (≤298 K) and addition of water to alcohol (≥10%) are very important factors for selective H_2O_2 formation. As shown in Figure 2a, photoreaction of an EtOH/water/O_2 system with g-C_3N_4 at ≤298 K produces H_2O_2 with high selectivity (~90%), but the selectivity decreases significantly at >298 K. This is due to the thermal decomposition of H_2O_2 at elevated temperature.[36] In addition, as shown in Figure 2b, photoreaction of g-C_3N_4 at 298 K without water shows very low H_2O_2 selectivity (63%),

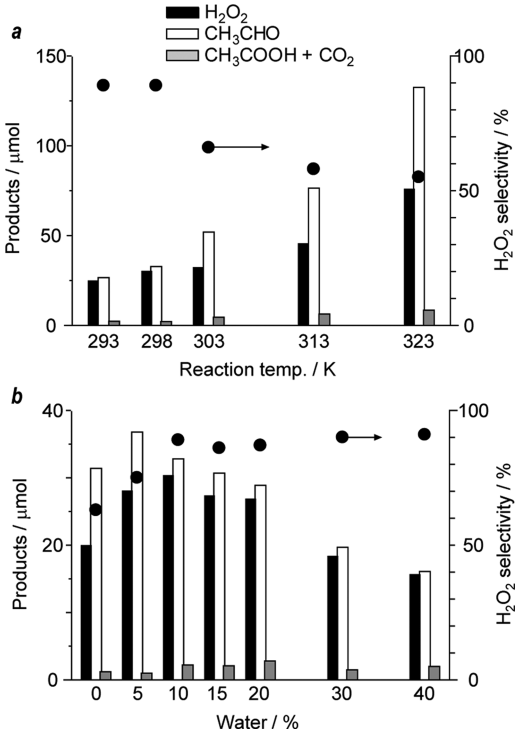

Figure 2. (a) Effect of reaction temperature on the amount of products and H_2O_2 selectivity during photoreaction with g-C_3N_4 in an EtOH/water/O_2 system. Reaction conditions are identical to those in Table 1. (b) Effect of water content in solution on the amount of products and H_2O_2 selectivity during photoreaction with g-C_3N_4 in an EtOH/O_2 system.

but it increases up to ~90% by the addition of ≥10% water. This is probably because the stabilization of H_2O_2 by the hydration with water molecules[37] suppresses decomposition of H_2O_2. These data suggest that photoreaction with water at around room temperature promotes selective H_2O_2 production.

Mechanism for selective H_2O_2 formation on the photoexcited g-C_3N_4 can be explained by Scheme 2. Photoexcitation of g-C_3N_4 by two photons (a) creates e^-−h^+ charge-separated state (b). The formed e^- are localized at the C1 and N4 positions of the triazine ring, whereas the h^+ are localized at the

dx.doi.org/10.1021/cs401208c | ACS Catal. 2014, 4, 774−780

Scheme 2. Proposed Mechanism for Selective H_2O_2 Formation on the Surface of Photoactivated g-C_3N_4

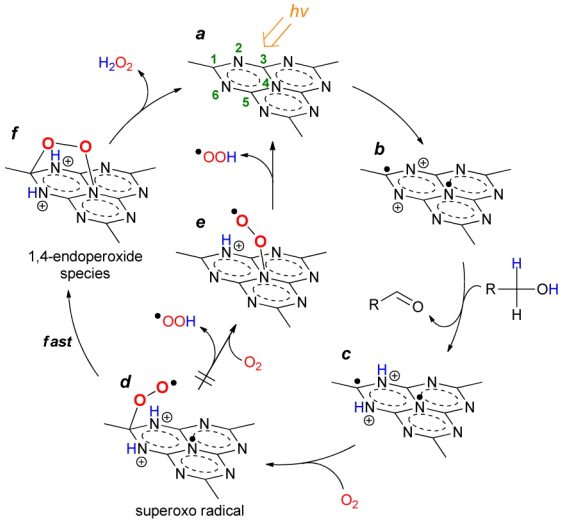

N2 and N6 positions.[38] The h^+ remove α- and β-hydrogens of alcohol and produce aldehyde (c).[31] The e^- on either C1 or N4 position reduces O_2 and produces a superoxo radical (d).[39] The radical is usually released as a superoxide (•OOH) radical (e) via the reaction with the proton, promoting one-electron reduction of O_2 (eq 3).[15] In contrast, on g-C_3N_4, the superoxo radical (d) is rapidly reduced by the e^- at the para position of the triazine ring, producing a 1,4-endoperoxide species (f).[40] Protonation of the endoperoxide species produces H_2O_2[15,41] and completes the photocatalytic cycle. These mechanisms indicate that selective H_2O_2 formation on the photoexcited g-C_3N_4 is due to the rapid formation of the 1,4-endoperoxide species (d → f). This suppresses one-electron reduction of O_2 (d → e → a) and selectively promotes two-electron reduction of O_2.

The suppression of one-electron reduction of O_2 (•OOH radical formation) on g-C_3N_4 is confirmed by ESR analysis with 5,5-dimethyl-1-pyrroline *N*-oxide (DMPO), a spin trapping reagent. Figure 3 shows the ESR spectra of the solution recovered after photoreaction of an EtOH/water/O_2 system with catalyst and DMPO. As shown in Figure 3a, the spectrum obtained after photoreaction with TiO_2 shows strong signals

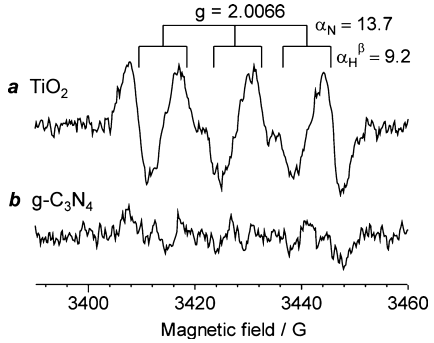

Figure 3. ESR spectra measured at 298 K for the solutions obtained by photoirradiation of (a) TiO_2 or (b) g-C_3N_4 in an EtOH/water/O_2 system. Reactions were carried out for 1 min under conditions identical to those in Table 1 with DMPO (0.1 mmol). The spectra obtained by 5 min irradiation are shown in Figure S6 (Supporting Information).

assigned to the DMPO−•OOH spin adduct (α_N = 13.7 G; α_H^β = 9.2 G, g = 2.0066).[42,43] This suggests that one-electron reduction of O_2 indeed occurs on TiO_2, resulting in very low selectivity for H_2O_2 production (Table 1, entry 1). In contrast, as shown in Figure 3b, the reaction with g-C_3N_4 shows only a very small adduct signal.[23,44] This suggests that, as shown in Scheme 2, the superoxo radical is rapidly reduced by another e^- (d → f), thus suppressing one-electron reduction of O_2 (d → e).

The formation of 1,4-endoperoxide species (Scheme 2f) on the photoactivated g-C_3N_4 is confirmed by Raman spectroscopy. As shown in Figure 4A, the g-C_3N_4 itself exhibits three

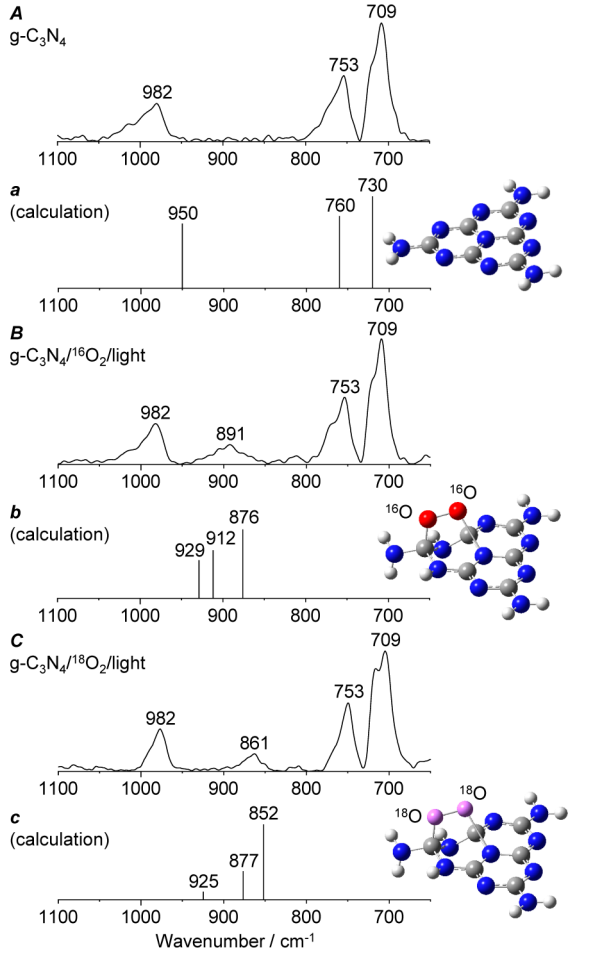

Figure 4. Raman spectra for (A) g-C_3N_4 and the sample recovered after photoreaction (12 h) of an EtOH/water mixture with (B) $^{16}O_2$ and (C) $^{18}O_2$. Calculated Raman shift for (a) the tri-*s*-triazine unit and the units with (b) ^{16}O−^{16}O and (c) ^{18}O−^{18}O 1,4-endoperoxide species. Calculations were performed at the DFT level with the B3LYP/6-31g(d) basis set. The white, gray, blue, red, and purple spheres represent H, C, N, ^{16}O, and ^{18}O atoms, respectively.

bands at 709, 753, and 982 cm^{-1}. Both 709 and 982 cm^{-1} bands are assigned to the breathing modes of triazine ring,[45] and the 753 cm^{-1} band is assigned to the out-of-plane bending mode of graphitic domains.[46] Figure 4a shows the Raman shift of the tri-*s*-triazine unit, obtained by ab initio calculation using the density functional theory (DFT) within the Gaussian 03 program. The obtained three bands (730, 760, and 950 cm^{-1}) are similar to the observed bands (Figure 4A), suggesting that DFT calculation precisely represents the electronic structure of

dx.doi.org/10.1021/cs401208c | *ACS Catal.* 2014, 4, 774−780

g-C_3N_4. Figure 4B shows the spectrum of the g-C_3N_4 recovered after photoreaction in an EtOH/water/$^{16}O_2$ system. A new broad band appears at 891 cm^{-1}. Figure 4b depicts the calculated Raman shift of the 1,4-endoperoxide species adsorbed on the tri-*s*-triazine unit. The obtained three bands (876, 912, and 929 cm^{-1}) are assigned to C1−^{16}O symmetric vibration, ^{16}O−^{16}O stretching vibration, and C1−^{16}O asymmetric vibration of the 1,4-endoperoxide species, respectively, and agree well with the observed broad band at 891 cm^{-1} (Figure 4B).

These data suggest that an endoperoxide species is indeed produced on the g-C_3N_4 surface. The endoperoxide formation is further confirmed by the spectrum of g-C_3N_4 recovered after photoreaction with labeled molecular oxygen ($^{18}O_2$). As shown in Figure 4C, the 891 cm^{-1} band disappears, and a new broad band appears at 861 cm^{-1}. DFT calculation of the ^{18}O−^{18}O endoperoxide species on g-C_3N_4 (Figure 4c) revealed that the isotopic shifts of the three bands are −24, −35, and −4 cm^{-1}, respectively, which are consistent with the observed shift (Δ = −30 cm^{-1}). These data suggest that, as shown in Scheme 2 (d → f), photoexcited g-C_3N_4 indeed produces 1,4-endoperoxide species via two-electron reduction of O_2. Almost no formation of $^{\bullet}$OOH radical (Scheme 2; d → e) is probably because the superoxo radical is rapidly reduced (d → f) due to the stabilization of endoperoxide species on the C1 and N4 positions of the triazine ring, as often observed for related anthracene systems.[47,48] This thus suppresses one-electron reduction of O_2, thus promoting selective two-electron reduction.

The proposed photoreaction mechanism (Scheme 2) involving the formation of endoperoxide species on the g-C_3N_4 surface and its transformation to H_2O_2 is supported by the photoreaction using g-C_3N_4 loaded with Pt nanoparticles ($Pt_{0.1}$/g-C_3N_4 and Pt_1/g-C_3N_4). As shown in Table 1 (entries 6, 7, and 8), increased Pt loadings enhance photooxidation of EtOH because of the enhanced charge separation by the transfer of conduction band e^- to Pt particles.[31] The increased Pt loadings, however, significantly decrease the H_2O_2 selectivity (<11%). This suggests that the g-C_3N_4 surface indeed behaves as the active site for two-electron reduction of O_2. In addition, as shown in Figure S7 (Supporting Information), the intensity of the Raman band for 1,4-endoperoxide species (891 cm^{-1}) on these catalysts decreases with the Pt loadings. These cross-relationships clearly suggest that, as shown in Scheme 2, the efficient formation of 1,4-endoperoxide species on the photoactivated g-C_3N_4 surface and its transformation to H_2O_2 promote highly selective formation of H_2O_2.

The g-C_3N_4 system successfully produces H_2O_2 even under sunlight irradiation. Figure 5b shows the time-dependent change in the amount of H_2O_2 formed and the H_2O_2 selectivity during photoreaction with g-C_3N_4 under sunlight exposure. As shown by the blue symbol, irradiation of the entire wavelength light (>300 nm) successfully produces H_2O_2, but the selectivity is only about 80% due to the subsequent photodecomposition of the formed H_2O_2 by absorbing UV light.[16] In contrast, irradiation with >420 nm light using a glass filter (orange symbol) produces H_2O_2 with high selectivity (>90%). These results indicate that the g-C_3N_4 system is successfully activated by the visible region light within sunlight and promotes selective production of H_2O_2.

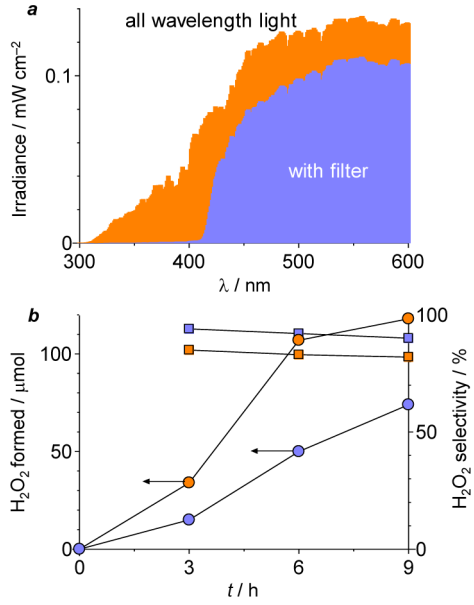

Figure 5. (a) Average spectral irradiance of sunlight and (b) time-dependent change in the amount of H_2O_2 and the selectivity during photoreaction of g-C_3N_4 in a 2-propanol/water/O_2 system under sunlight exposure (orange) without filter and (blue) with filter (λ > 420 nm). Photoreaction was performed at 8:00−17:00 (north latitude 34.7°, east longitude 135.5°).

CONCLUSION

We found that g-C_3N_4 activated by visible light irradiation (>420 nm) in water with alcohol and O_2 produces H_2O_2 with very high selectivity. Photoexcited g-C_3N_4 promotes selective two-electron reduction of O_2 due to the efficient formation of 1,4-endoperoxide species on its surface. This suppresses one-electron reduction of O_2 and promotes selective production of H_2O_2. Sunlight activation of g-C_3N_4 also successfully promotes selective H_2O_2 production. At present, the photocatalytic activity of g-C_3N_4 is low; the amount of H_2O_2 formed by 12 h of reaction is only 30 μmol. The activity, however, would be improved by using g-C_3N_4 materials with high surface area synthesized by polymerization of urea[49] or silica-templated polymerization of cyanamide.[27] The present photoprocess has significant advantages: (i) inexpensive metal-free photocatalyst, (ii) cost-free light source (sunlight), (iii) safe hydrogen source (alcohol), and (iv) mild reaction conditions (atmospheric pressure and ambient temperature). The basic concept presented here, based on selective two-electron reduction of O_2 on the photoactivated g-C_3N_4 surface, may contribute to the design of more efficient photocatalytic systems for H_2O_2 production and may open a new strategy toward organic synthesis driven by sunlight.

EXPERIMENTAL SECTION

g-C_3N_4.[27] Cyanamide (9.0 g) was added to a porcelain cup and calcined under N_2 flow at 823 K for 4 h with the heating rate being 2.3 K min^{-1}. Grinding of the resultant affords yellow powders of g-C_3N_4 (6.8 g).

Pt_1/TiO_2.[50] TiO_2 (1.0 g) was added to water (20 mL) containing $H_2PtCl_6{\cdot}6H_2O$ (26.8 mg). Solvents were removed by evaporation at 353 K with vigorous stirring. The obtained powders were calcined under air flow and then reduced under H_2 flow at 673 K. The heating rate was 2 K min^{-1}, and the holding time at 673 K was 2 h.

dx.doi.org/10.1021/cs401208c | ACS Catal. 2014, 4, 774−780

Au_1/TiO_2.[32] TiO_2 (1.0 g) was added to water (50 mL) containing $HAuCl_4 \cdot 4H_2O$ (22.9 mg). The pH of the solution was adjusted to ~7 with 1 mM NaOH, and the solution was stirred at 353 K for 3 h. The particles were recovered by centrifugation, washed with water, and dried at 353 K for 12 h. The powders were calcined under air flow, for which the heating rate was 2 K min^{-1} and the holding time at 673 K was 2 h.

F-TiO_2.[13] TiO_2 (20 mg) was added to an EtOH/water mixture (9/1 v/v, 5 mL) containing NaF (0.1 mol L^{-1}) within a Pyrex glass tube (φ 12 mm; capacity, 20 mL). The solution was then used for photocatalytic reaction.

N-TiO_2.[51] Tetraisopropyl titanate (35 mL) was added to an ammonia solution (~28 wt %, 100 mL) and stirred vigorously at room temperature for 12 h. The resultant precipitate was washed thoroughly with water and recovered by filtration. The obtained powders were dried at 343 K for 12 h and calcined at 673 K for 3 h under air flow.

$Pt_x/g\text{-}C_3N_4$. g-C_3N_4 (1.0 g) was added to water (40 mL) containing $H_2PtCl_6 \cdot 6H_2O$ [2.7 mg (x = 0.1) or 26.8 mg (x = 1.0)]. Solvents were removed by evaporation at 353 K with vigorous stirring. The obtained powders were reduced under H_2 flow at 573 K for 2 h with the heating rate being 2 K min^{-1}.

Photoreaction. Catalyst (20 mg) was added to an alcohol/water mixture (9/1 v/v, 5 mL) within a Pyrex glass tube (φ 12 mm; capacity, 20 mL), and the tube was sealed with a rubber septum cap. The catalyst was dispersed well by ultrasonication for 3 min, and O_2 was bubbled through the solution for 5 min. The tube was immersed in a temperature-controlled water bath and photoirradiated at λ > 420 nm using a 2 kW Xe lamp (USHIO Inc.) with magnetic stirring.[35] The light intensity at 420−500 nm was 26.9 W m^{-2}. Sunlight reactions were performed on October 14, 2013 at 8:00−17:00 at the top of the laboratory building (north latitude 34.7°, east longitude 135.5°). The light intensities at 300−500 nm and at 420−500 nm were 8.0 and 4.1 mW cm^{-2}, respectively. The highest temperature of the solution during reaction was 303 K. After the reaction, the gas-phase product was analyzed by GC−TCD (Shimadzu; GC-14B). The catalyst was recovered by centrifugation, and the liquid-phase products were analyzed by GC−FID (GC-2010 system). The H_2O_2 amount was determined by redox titration with $KMnO_4$.[43] Spectral irradiance for the light source was measured with a spectroradiometer USR-40 (USHIO Inc.).

Action Spectrum Analysis. Photoreactions were carried out using an EtOH/water mixture (9/1 v/v, 3 mL) and g-C_3N_4 (12 mg) within a Pyrex glass tube (φ 12 mm; capacity, 20 mL). After ultrasonication and O_2 bubbling, the tube was photoirradiated using a Xe lamp for 3 h, for which the incident light was monochromated by the band-pass glass filters (Asahi Techno Glass Co.).[32] The full-width at half-maximum of the light was 11−16 nm. Photodecomposition of H_2O_2 was carried out in water (3 mL) containing H_2O_2 (6 mM) within a Pyrex glass tube. After O_2 bubbling, the tube was irradiated by a monochromated light using a Xe lamp for 3 h.

Calculation Details. All calculations were performed at the DFT level within the Gaussian 03 program using the B3LYP/6-31G(d) basis set. Cartesian coordinates for the tri-*s*-triazine unit and the unit with 1,4-endoperoxide species are summarized in Supporting Information.

Raman Spectroscopy. The spectra were measured on a confocal Raman microscope (LabRAM HR-800, HORIBA).[15] YAG laser (784 nm line) was used as the excitation source, where the laser power was 100 mW and the total data accumulation time was 15 s. The samples were prepared as follows: After photoreaction, g-C_3N_4 samples were recovered by centrifugation and dried at room temperature in vacuo. They were mounted on a microscope slide and subjected to analysis.

ESR Measurement. The spectra were recorded at the X-band using a Bruker EMX-10/12 spectrometer with a 100 kHz magnetic field modulation at a microwave power level of 10.5 mW, where microwave power saturation of the signals does not occur.[15] The magnetic field was calculated using a using a 1,1-diphenyl-2-picrylhydrazyl (DPPH) as standard. The measurement was carried out as follows: catalyst (20 mg) was suspended in an EtOH/water mixture (9/1 v/v, 5 mL) and DMPO (0.10 mmol) within a Pyrex glass tube (φ12 mm; capacity, 20 mL), and the tube was sealed with a rubber septum cap. After ultrasonication (3 min) and O_2 bubbling (5 min), the solution was photoirradiated (λ > 420 nm) with stirring. The catalyst was recovered by centrifugation, and the resulting solution was subjected to analysis.

Other Analysis. Diffuse-reflectance UV−vis spectra were measured on a UV−vis spectrophotometer (JASCO Corp.; V-550) equipped with Integrated Sphere Apparatus ISV-469, using $BaSO_4$ as a reference. XRD patterns were measured on a Philips X'Pert-MPD spectrometer. XPS analysis was performed using a JEOL JPS-9000MX spectrometer with Mg Kα radiation as the energy source. TEM observations were performed using an FEI Tecnai G2 20ST analytical electron microscope operated at 200 kV.[52]

■ ASSOCIATED CONTENT

Ⓢ Supporting Information

Photoreaction results with various alcohols (Table S1); XRD pattern (Figure S1), XPS chart (Figure S2), and TEM image (Figure S3) of g-C_3N_4; Size distribution of metal particles (Figure S4); Time-dependent change in H_2O_2 formation (Figure S5); ESR spectra for spin adduct (Figure S6); Raman spectra for endoperoxide species on various catalysts (Figure S7); Cartesian coordinates for tri-*s*-triazine unit and the unit with 1,4-endoperoxide species. This material (PDF) is available free of charge via the Internet at http://pubs.acs.org.

■ AUTHOR INFORMATION

Corresponding Author

*E-mail: shiraish@cheng.es.osaka-u.ac.jp.

Notes

The authors declare no competing financial interest.

■ ACKNOWLEDGMENTS

This work was supported by a Grant-in-Aid for Scientific Research (No. 23360349) from the Ministry of Education, Culture, Sports, Science and Technology, Japan (MEXT).

■ REFERENCES

(1) Campos-Martin, J. M.; Blanco-Brieva, G.; Fierro, J. L. G. *Angew. Chem., Int. Ed.* **2006**, *45*, 6962−6984.
(2) Lunsford, J. H. *J. Catal.* **2003**, *216*, 455−460.
(3) Blanco-Brieva, G.; Cano-Serrano, E.; Campos-Martin, J. M.; Fierro, J. L. G. *Chem. Commun.* **2004**, 1184−1185.
(4) Melada, S.; Rioda, R.; Menegazzo, F.; Pinna, F.; Strukul, G. *J. Catal.* **2006**, *239*, 422−430.
(5) Choudhary, V. R.; Gaikwad, A. G.; Sansare, S. D. *Angew. Chem., Int. Ed.* **2001**, *40*, 1776−1779.

(6) Landon, P.; Collier, P. J.; Papworth, A. J.; Kiely, C. J.; Hutchings, G. J. *Chem. Commun.* **2002**, 2058−2059.
(7) Edwards, J. K.; Solsona, B.; Ntainjua, E.; Carley, A. F.; Herzing, A. A.; Kiely, C. J.; Hutchings, G. J. *Science* **2009**, *323*, 1037−1041.
(8) Kormann, C.; Bahnemann, D. W.; Hoffmann, M. R. *Environ. Sci. Technol.* **1988**, *22*, 798−806.
(9) Cai, R.; Kubota, Y.; Fujishima, A. *J. Catal.* **2003**, *219*, 214−218.
(10) Goto, H.; Hanada, Y.; Ohno, T.; Matsumura, M. *J. Catal.* **2004**, *225*, 223−229.
(11) Hirakawa, T.; Nosaka, Y. *J. Phys. Chem. C* **2008**, *112*, 15818−15823.
(12) Maurino, V.; Minero, C.; Mariella, G.; Pelizzetti, E. *Chem. Commun.* **2005**, 2627−2629.
(13) Teranishi, M.; Naya, S.; Tada, H. *J. Am. Chem. Soc.* **2010**, *132*, 7850−7851.
(14) Tsukamoto, D.; Shiro, A.; Shiraishi, Y.; Sugano, Y.; Ichikawa, S.; Tanaka, S.; Hirai, T. *ACS Catal.* **2012**, *2*, 599−603.
(15) Shiraishi, Y.; Kanazawa, S.; Tsukamoto, D.; Shiro, A.; Sugano, Y.; Hirai, T. *ACS Catal.* **2013**, *3*, 2222−2227.
(16) Goldstein, S.; Aschengrau, D.; Diamant, Y.; Rabani, J. *Environ. Sci. Technol.* **2007**, *41*, 7486−7490.
(17) Wang, X.; Maeda, K.; Thomas, A.; Takanabe, K.; Xin, G.; Carlsson, J. M.; Domen, K.; Antonietti, M. *Nat. Mater.* **2009**, *8*, 76−80.
(18) Thomas, A.; Fischer, A.; Goettmann, F.; Antonietti, M.; Müller, J. O.; Schlögl, R.; Carlsson, J. M. *J. Mater. Chem.* **2008**, *18*, 4893−4908.
(19) Schwinghammer, K.; Tuffy, B.; Mesch, M. B.; Wirnhier, E.; Martineau, C.; Taulelle, F.; Schnick, W.; Senker, J.; Lotsch, B. V. *Angew. Chem., Int. Ed.* **2013**, *52*, 2435−2439.
(20) Cui, Y.; Ding, Z.; Liu, P.; Antonietti, M.; Fu, X.; Wang, X. *Phys. Chem. Chem. Phys.* **2012**, *14*, 1455−1462.
(21) Zhang, J.; Chen, X.; Takanabe, K.; Maeda, K.; Domen, K.; Epping, J. D.; Fu, X.; Antonietti, M.; Wang, X. *Angew. Chem., Int. Ed.* **2010**, *49*, 441−444.
(22) Abe, R.; Takami, H.; Murakami, N.; Ohtani, B. *J. Am. Chem. Soc.* **2008**, *130*, 7780−7781.
(23) Su, F.; Mathew, S. C.; Lipner, G.; Fu, X.; Antonietti, M.; Blechert, S.; Wang, X. *J. Am. Chem. Soc.* **2010**, *132*, 16299−16301.
(24) Li, X.-H.; Chen, J.-S.; Wang, X.; Sun, J.; Antonietti, M. *J. Am. Chem. Soc.* **2011**, *133*, 8074−8077.
(25) Li, X.-H.; Wang, X.; Antonietti, M. *ACS Catal.* **2012**, *2*, 2082−2086.
(26) Chen, Y.; Zhang, J.; Zhang, M.; Wang, X. *Chem. Sci.* **2013**, *4*, 3244−3248.
(27) Wang, X.; Maeda, K.; Chen, X.; Takanabe, K.; Domen, K.; Hou, Y.; Fu, X.; Antonietti, M. *J. Am. Chem. Soc.* **2009**, *131*, 1680−1681.
(28) Ji, H.; Chang, F.; Hu, X.; Qin, W.; Shen, J. *Chem. Eng. J.* **2013**, *218*, 183−190.
(29) Li, X.; Zhang, J.; Shen, L.; Ma, Y.; Lei, W.; Cui, Q.; Zou, G. *Appl. Phys. A: Mater. Sci. Process.* **2009**, *94*, 387−392.
(30) Xu, H.; Yan, J.; Xu, Y.; Song, Y.; Li, H.; Xia, J.; Huang, C.; Wan, H. *Appl. Catal., B* **2013**, *129*, 182−193.
(31) Shiraishi, Y.; Sugano, Y.; Tanaka, S.; Hirai, T. *Angew. Chem., Int. Ed.* **2010**, *49*, 1656−1660.
(32) Tsukamoto, D.; Shiraishi, Y.; Sugano, Y.; Ichikawa, S.; Tanaka, S.; Hirai, T. *J. Am. Chem. Soc.* **2012**, *134*, 6309−6315.
(33) Asahi, R.; Morikawa, T.; Ohwaki, T.; Aoki, K.; Taga, Y. *Science* **2001**, *293*, 269−271.
(34) Liu, J.; Zhang, Y.; Lu, L.; Wu, G.; Chen, W. *Chem. Commun.* **2012**, *48*, 8826−8828.
(35) Sugano, Y.; Shiraishi, Y.; Tsukamoto, D.; Ichikawa, S.; Tanaka, S.; Hirai, T. *Angew. Chem., Int. Ed.* **2013**, *52*, 5295−5299.
(36) Rice, F. O.; Reiff, O. M. *J. Phys. Chem.* **1927**, *31*, 1352−1356.
(37) Izgorodin, A.; Izgorodina, E.; MacFarlane, D. R. *Energy Environ. Sci.* **2012**, *5*, 9496−9501.
(38) Huda, M. N.; Turner, J. A. *J. Appl. Phys.* **2010**, *107*, 123703−123703-5.
(39) Nakamura, R.; Imanishi, A.; Murakoshi, K.; Nakato, Y. *J. Am. Chem. Soc.* **2003**, *125*, 7443−7450.
(40) Fidder, H.; Lauer, A.; Freyer, W.; Koeppe, B.; Heyne, K. *J. Phys. Chem. A* **2009**, *113*, 6289−6296.
(41) Zhang, M.; Wang, Q.; Chen, C.; Zang, L.; Ma, W.; Zhao, J. *Angew. Chem., Int. Ed.* **2009**, *48*, 6081−6084.
(42) Harbour, J. R.; Hair, M. L. *J. Phys. Chem.* **1978**, *82*, 1397−1399.
(43) Tsukamoto, D.; Ikeda, M.; Shiraishi, Y.; Hara, T.; Ichikuni, N.; Tanaka, S.; Hirai, T. *Chem.—Eur. J.* **2011**, *17*, 9816−9824.
(44) Zhang, P.; Wang, Y.; Li, H.; Antonietti, M. *Green Chem.* **2012**, *14*, 1904−1908.
(45) Zinin, P. V.; Ming, L. C.; Sharma, S. K.; Khabashesku, V. N.; Liu, X.; Hong, S.; Endo, S.; Acosta, T. *Chem. Phys. Lett.* **2009**, *472*, 69−73.
(46) Papadimitriou, D.; Roupakas, G.; Dimitriadis, C. A.; Logothetidis, S. *J. Appl. Phys.* **2002**, *92*, 870−875.
(47) Lauer, A.; Dobryakov, A. L.; Kovalenko, S. A.; Fidder, H.; Heyne, K. *Phys. Chem. Chem. Phys.* **2011**, *13*, 8723−8732.
(48) Kupfer, S.; Pérez-Hernández, G.; González, L. *Theor. Chem. Acc.* **2012**, *131*, 1295−1295−14.
(49) Zhang, Y.; Liu, J.; Wu, G.; Chen, W. *Nanoscale* **2012**, *4*, 5300−5303.
(50) Shiraishi, Y.; Sakamoto, H.; Sugano, Y.; Ichikawa, S.; Hirai, T. *ACS Nano* **2013**, *7*, 9287−9297.
(51) Higashimoto, S.; Takamatsu, K.; Azuma, M.; Kitano, M.; Matsuoka, M.; Anpo, M. *Catal. Lett.* **2008**, *122*, 33−36.
(52) Shiraishi, Y.; Tanaka, K.; Shirakawa, E.; Sugano, Y.; Ichikawa, S.; Tanaka, S.; Hirai, T. *Angew. Chem., Int. Ed.* **2013**, *52*, 8304−8308.